Simulated Moving-Bed Units with Extra-Column Dead Volume

Cristiano Migliorini and Marco Mazzotti
ETH Zürich, Insitut für Verfahrenstechnik, Sonneggstrasse 3, CH-8092 Zürich, Switzerland

Massimo Morbidelli
ETH Zürich, Laboratorium für Technische Chemie LTC, Universitätstrasse 6, CH-8092 Zürich, Switzerland

Simulated moving-bed (SMB) technology is attracting increased interest for application to the separation of pharmaceuticals and fine chemicals, particularly to enantioseparations. Unlike the large-scale UOP Sorbex process, these small-scale units use a series of HPLC columns, and the volume of the connecting lines may become comparable to the volume of the columns. In this work the effect of extra-column dead volume on SMB performance is analyzed, with the aim of providing a conceptual framework to account for it. In particular, guidelines to design SMB operating conditions with non-negligible extra-column dead volumes to achieve the desired separation performance are provided. These are quantitatively assessed through comparison with the results obtained using a detailed SMB model, which accounts for extra-column dead volumes. The model allows the extent and the role of extra-column band broadening due to the presence of dead volumes to be evaluated. A set of experimental results on a laboratory SMB unit is discussed in light of the theoretical findings.

Introduction

The simulated moving-bed (SMB) technology illustrated in Figure 1 has been applied since the 1960s by Universal Oil Products for large-scale separations in the petrochemical industry, and today the so-called Sorbex processes, such as Parex and Molex, are standard unit operations for the separation of *p*-xylene from aromatics and *n*-paraffins from branched and cyclic hydrocarbons. This technology is also applied to large-scale separations in the food industry, mainly for separating fructose from high-fructose corn syrup (Sarex process) (Johnson and Kabza, 1993). All these processes are operated in the liquid phase, but feasibility of some of these separations in the vapor-phase SMB also has been demonstrated (Storti et al., 1992; Mazzotti et al., 1996a).

In the last few years the development of stable and efficient chiral stationary phases for HPLC chromatography has encouraged the application of preparative batch chromatography for the separation of enantiomers. The demand for optically pure compounds and the need to avoid the drawbacks of batch chromatography (high dilution of the products, low productivity per unit mass of the stationary phase, and difficult optimization of the process) justify the increasing interest in the application of the SMB technology to small-scale separations in the fine-chemical and pharmaceutical industries. Moreover, the scale-up of a separation from the analytical scale to the preparative SMB separation is fast, since the same mobile and stationary phases can be used. This allows a reduction in the time from the discovery of a new drug to when it comes on the market. As a further advantage with respect to batch chromatography, it has been proved by numerical (Migliorini et al., 1999) and experimental results (Pedeferri et al., 1999) that SMB performance is rather insensitive to column efficiency. In fact, in SMBs it is possible to achieve high purities even when the resolution on a single column is below 1, that is, the separation is not achieved under analytical conditions. This is due to the countercurrent contact between the stationary and the mobile phase obtained in SMB units.

The technical realization of the large-scale Sorbex process involves a single vessel, divided in a number of subsections, usually 12 (Johnson and Kabza, 1993). This solution is not convenient in the small scale, where SMBs are constituted of

Correspondence concerning this article should be addressed to M. Morbidelli.

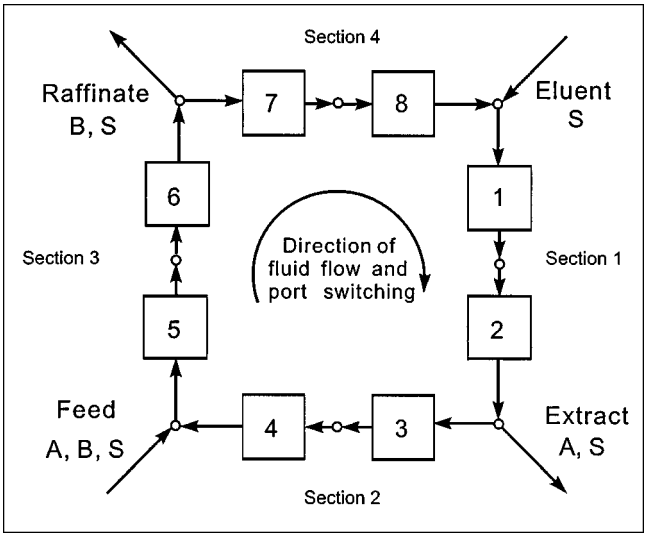

Figure 1. Simulated moving-bed unit for continuous chromatographic separations, with column configuration 2-2-2-2.

Each of the eight subsections represents a chromatographic module with or without extra-column dead volume (see Figure 2).

a set of columns properly connected by a system of valves and tubing. In these kinds of SMB units the extra-column dead volumes, though carefully kept to a minimum, become comparable to the column volume and cannot be neglected, in particular when designing the operating conditions. The importance of accounting for this effect has already been recognized in the literature (Yun et al., 1997; Wu et al., 1998), but no detailed analysis, either experimental or theoretical, has been reported. The common opinion is that extra-column dead volumes hinder high separation performance, by introducing harmful extra-column band broadening.

The objective of this work is to fill this gap by studying the effect of dead volumes on the performance of SMB units. To this end, a detailed model of the SMB unit accounting for extra-column dead volumes is developed in the following section. In the fourth section the results obtained with such a model are discussed in light of the theoretical analysis developed in the third section, which provides guidelines for the design of operating conditions in SMBs with nonnegligible extra-column dead volume. Finally, all these theoretical and numerical findings are assessed by discussing experimental results relative to the separation of the Tröger's base enantiomers on microcrystalline triacetylcellulose, in an 8-column SMB unit where the extra-column dead volume is 40% of the column volume (Pedeferri et al., 1999).

Modeling SMB Units with Extra-Column Dead Volume

The SMB model proposed in this work is based on the equilibrium-dispersive model of chromatographic columns. Its advantages and drawbacks have been discussed elsewhere (Migliorini et al., 1999), so here only a brief description of the basic equations is given together with a discussion of the approach adopted for modeling extra-column dead volumes.

Column model

The simplest model of chromatographic columns is the ideal model, where mass-transfer resistance and axial dispersion are neglected. The column efficiency is assumed to be infinite, and thermodynamic equilibrium between the mobile and stationary phases is enforced, hence (see the Notation section for symbols)

$$n_i = f_i^{\mathrm{eq}}(c). \tag{1}$$

The resulting model equations are a system of first-order hyperbolic partial differential equations that can be solved analytically in the frame of the so-called Equilibrium Theory, whenever linear or constant selectivity Langmuir isotherms are considered (Helferrich and Klein, 1970; Rhee et al., 1970).

In the equilibrium-dispersive model a second-order term is added, which accounts in a lumped way for finite column efficiency due to axial dispersion and finite mass-transfer resistance. The mass balance for component i can be cast as follows

$$\epsilon^* \frac{\partial c_i}{\partial t} + (1-\epsilon^*)\frac{\partial n_i}{\partial t} + u\frac{\partial c_i}{\partial z} = \epsilon^* D_{\mathrm{ap},i}\frac{\partial^2 c_i}{\partial z^2}. \tag{2}$$

The numerical solution of the model can be obtained by discretizing the first-order space derivative with a backward finite difference scheme that introduces an error proportional to the dispersive term (Guiochon et al., 1994). The relationship between the number of space intervals and the axial dispersion coefficient in Eq. 2 is

$$N_C = \frac{Lu}{2\epsilon^* D_{\mathrm{ap}}}. \tag{3}$$

Modeling the extra-column dead volume

In this work a model is implemented that accounts for the effects of extra-column dead volume. The flow in the dead volume is described with a second-order model according to the following equation

$$\frac{\partial c_i}{\partial t} + u\frac{\partial c_i}{\partial z} = D_D\frac{\partial^2 c_i}{\partial z^2}. \tag{4}$$

This allows us to account for mixing effects in the dead volume itself in a rather flexible way. The numerical solution of this model is similar to that of the column model. Therefore, the first-order derivative is approximated with a backward finite difference that introduces a numerical error proportional to the second-order term; the number of grid points used to discretize the dead volume, which is equal to the number of mixing stages, is related to the dispersion coefficient of Eq. 4 through the relationship

$$N_D = \frac{L_D u}{2D_D}. \tag{5}$$

By changing the dispersion coefficient, that is, the number of grid points in Eq. 5, it is possible to tune the effect of mixing

in the dead volume. At a large number of grid points plug flow with negligible mixing is attained, whereas in the limit of infinite diffusion, that is, a single mixing stage, the extra-column dead volume behaves like a perfectly stirred tank. When V^D is very small compared to the volume of the columns, the residence time in the mixing units is much smaller than that in the chromatographic columns. Thus, the model is rather stiff from the numerical point of view, and the computational effort rather laborious.

SMB model

The SMB unit can be modeled as a closed loop of chromatographic modules, as illustrated in Figure 1, where a 2-2-2-2 configuration has been considered. Each chromatographic module (see Figure 2) consists of three parts: two empty dead volumes and the chromatographic column. The dead volumes are assumed to be located at the beginning and at the end of the column. Since the theoretical analysis in the following section shows that the actual distribution of the dead volumes has no influence on the results, the layout in Figure 2 is as general as any other with an overall dead volume of V^D. After space discretization, the model of a chromatographic module is made of a system of ordinary differential equations that account for both the dead volume and the chromatographic column. The chromatographic module models are coupled through the mass balances at the nodes between adjacent modules, which also involve the inlet and outlet streams to the unit (see Figure 1). When the integration time is equal to an integer multiple of the switch time t^*, the position of the inlet and outlet ports is shifted forward in the direction of the fluid flow. Then a new integration in time is started, using as the new initial condition the composition profile reached before the switch occurring at t^*.

Theoretical Background

Physical insight suggests that extra-column dead volume has an effect on increasing the residence time in the module made of the dead volume and the chromatographic column with respect to the retention time in the column alone (see Figure 2) and on spreading the concentration profiles in the SMB unit due to additional back mixing in the dead volume itself. The former effect can be dealt with in a rigorous fashion through the approach presented in this section and based on the Equilibrium Theory model, where mass-transfer resistance and axial mixing are neglected. The results obtained in this section allow us to extend the robust and optimal design criteria for the operating conditions of the SMB units referred to as ''Triangle Theory'' to the case where extra-column dead volumes cannot be neglected (Storti et al., 1993, 1995; Mazzotti et al., 1994, 1996b, 1997a,b; Chiang, 1998a, 1998b; Gentilini et al., 1998). These criteria are given in the cited works in terms of the flow rate ratios, m_j, $j = 1, \ldots, 4$, defined as follows

$$m_j = \frac{Q_j t^* - V\epsilon^*}{V(1-\epsilon^*)}. \tag{6}$$

The discussion will be presented following two different approaches based on different viewpoints; these lead to the same conclusions, thus yielding a procedure that can be adopted in the general case.

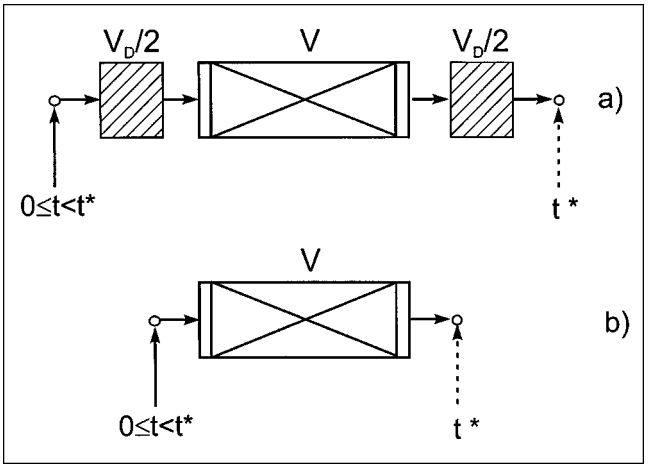

Figure 2. Chromatographic module of an SMB unit, with (a) and without (b) dead volumes.

The solid arrow indicates the position of an inlet stream in the time $0 \le t \le t^*$; the broken arrow indicates its position after the switch occurring at $t = t^*$.

Simulated moving bed

First, let us consider an SMB unit where the components to be separated are simply characterized by linear adsorption equilibria

$$n_i = H_i c_i. \tag{7}$$

The separation of interest is between species A and B, where $H_B < H_A$, that is, A and B are the more and less retained components, respectively. The residence time in the module illustrated in Figure 2 is composed of two contributions, the first given by the residence time in the extra-column dead volume, which in general may be different in the different sections of the unit, and the second by the retention time in the chromatographic column

$$t^r_{i,j} = t^D_j + t^R_{i,j} = \frac{V^D_j}{Q_j} + \frac{V\epsilon^*}{Q_j}\left[1 + \frac{1-\epsilon^*}{\epsilon^*}H_i\right], \qquad (i = A, B; \quad j = 1, \ldots, 4). \tag{8}$$

It is rather obvious that under the previous assumptions $t^r_{B,j} < t^r_{A,j}$.

Complete separation of A and B and regeneration of sections 1 and 4 of the SMB unit require that the following constraints be fulfilled

$$\text{Section 1:} \quad t^r_{A,1} \le t^*, \tag{9}$$

$$\text{Section 2:} \quad t^r_{B,2} \le t^* \le t^r_{A,2}, \tag{10}$$

$$\text{Section 3:} \quad t^r_{B,3} \le t^* \le t^r_{A,3}, \tag{11}$$

$$\text{Section 4:} \quad t^* \le t^r_{B,4}. \tag{12}$$

Using Eq. 8, these inequalities can be recast in the following

form

$$H_A \le \overline{m}_1, \tag{13}$$

$$H_B \le \overline{m}_2 \le H_A, \tag{14}$$

$$H_B \le \overline{m}_3 \le H_A, \tag{15}$$

$$\overline{m}_4 \le H_B, \tag{16}$$

where the modified flow rate ratio $\overline{m}_j$ is defined as follows

$$\overline{m}_j = \frac{Q_j t^* - V\epsilon^*}{V(1-\epsilon^*)} - \frac{V_j^D}{V(1-\epsilon^*)} = m_j - m_j^D, \tag{17}$$

and on the righthand side of Eq. 17 m_j is defined by Eq. 6 and $m_j^D = V_j^D/(V(1-\epsilon^*))$.

Equations 13 to 16 are structurally the same as those already reported in the literature for linear systems (Ruthven and Ching, 1989; Storti et al., 1993; Charton and Nicoud, 1995), but are now able to properly account for the effect of extra-column dead volume through the new term m_j^D. It is evident that whenever the V_j^D are so small as to be negligible the preceding equations reduce to the classic ones involving the parameters m_j only. Based on physical arguments, Eq. 17 was used before (Kniep, 1997).

The extension of these results to SMB separations characterized by nonlinear adsorption equilibria can be accomplished only in a special case, which is reported in the Appendix.

TCC Equivalence: Nonlinear Equilibria

The SMB technique was developed with the aim of finding a technologically feasible realization of an adsorptive countercurrent separator (Ruthven and Ching, 1989). Thus, in an SMB unit the countercurrent movement between the solid and the fluid phases is simulated in a discrete way, by periodically shifting the inlet and outlet ports of the unit. The equivalence between a true countercurrent unit (TCC), such as the one illustrated in Figure 3, and an SMB configuration has both conceptual and practical importance, since it can be exploited for modeling and design purposes. As a matter of fact, the design problem for TCC units can be solved in the frame of Equilibrium Theory for a rather large class of systems described by many nonlinear adsorption isotherms of applicative interests, such as the Langmuir (Storti et al., 1993; Mazzotti et al., 1996b), modified Langmuir (Mazzotti et al., 1997a), and bi-Langmuir adsorption isotherm (Gentilini et al., 1998), both in the binary (Mazzotti et al., 1997a) and in the multicomponent case (Mazzotti et al., 1994; Storti et al., 1995; Chiang, 1998a, 1998b). These results are given in the TCC unit in terms of the flow-rate ratios, m_j^{TCC} ($j = 1, \ldots, 4$), which are defined as

$$m_j^{\mathrm{TCC}} = \frac{Q_j^{\mathrm{TCC}} - Q_s\epsilon_p}{Q_s(1-\epsilon_p)}, \tag{18}$$

where Q_j^{TCC} and Q_s are the fluid and the solids flow rate, respectively. As an example of an application of this approach, the complete separation region in the (m_2, m_3) plane

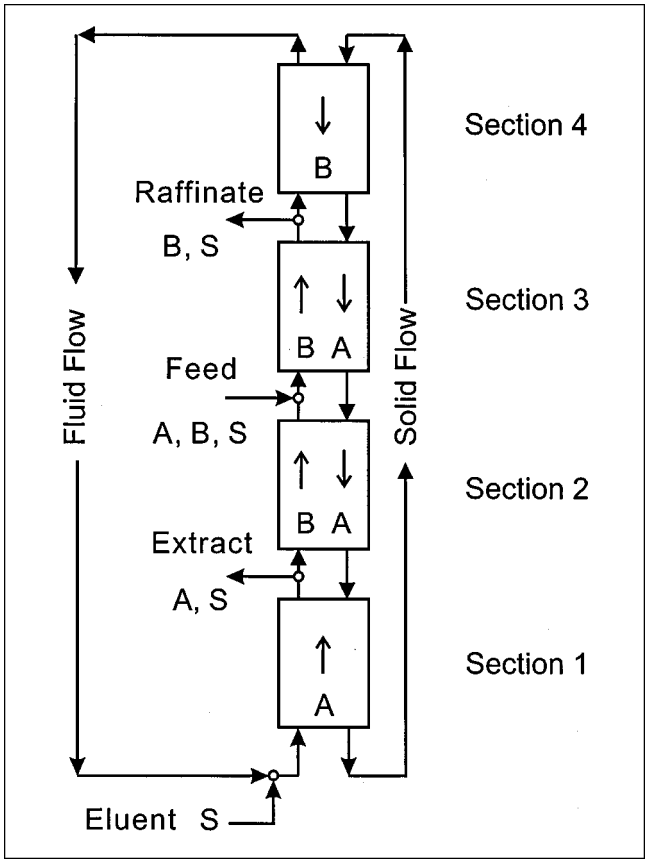

Figure 3. Four-section true countercurrent unit for continuous chromatographic separations.

for the separation of a binary mixture characterized by a Langmuir isotherm using a nonadsorbable desorbent, is illustrated in Figure 4.

The results obtained through the Equilibrium Theory for TCC units can be applied to SMB units by exploiting their equivalence. In fact, the two unit configurations achieve the same separation performances provided geometric and kinematic conversion rules given by the following relationships are fulfilled (Ruthven and Ching, 1989; Storti et al., 1992)

$$\frac{V}{t^*} = \frac{Q_s}{1-\epsilon_b} \tag{19}$$

$$Q_j = \left[Q_j^{\mathrm{TCC}} + \frac{Q_s\epsilon_b}{1-\epsilon_b} \right], \tag{20}$$

where Q_j, with no superscript, refers to the SMB unit, as in all previous equations. Using Eqs. 19 and 20, it can be readily shown that the definition of m_j^{TCC} (Eq. 18) reduces to that of m_j for SMB units given by Eq. 6. It follows that a result such as the one illustrated in Figure 4, which has been obtained by considering a TCC configuration and using the corresponding definition of m_j^{TCC}, that is, Eq. 18, can be directly applied to SMB units by interpreting the coordinates of the diagram according to the definition of m_j that is, Eq. 6.

The preceding results summarize the state of the art, where no account of extra-column dead volume is made. Before

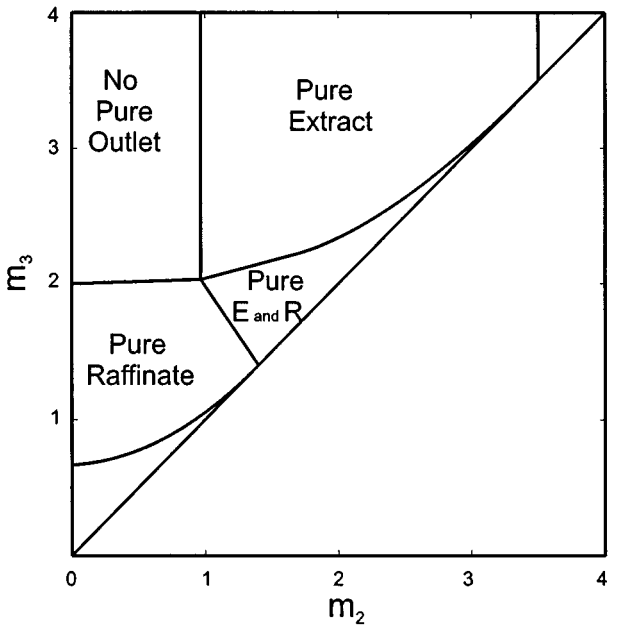

Figure 4. Separation of a two-component mixture using a nonadsorbable desorbent.

Regions of the (m_2, m_3) plane with different separation regimes in terms of the purity of the outlet streams, for a system described by the nonstoichiometric Langmuir isotherm of Eq. 22.

looking for a possible extension, it is worth reconsidering the conversion rules (Eqs. 19 and 20) in order to better understand how they are obtained. Let us consider the fixed-bed column of Figure 2b, which is part of the jth section of an SMB unit and has no extra-column dead volume. At time zero an inlet port is located in front of the column, whereas after a time period t^* this port is shifted to the node immediately behind the column. The fluid flow rate with respect to this inlet port, taken as a reference point, is made of two terms: a positive contribution due to the continuous fluid flow, with flow rate Q_j, and a negative contribution caused by the discrete jump of the whole column to the left of the inlet port, which occurs at time t^*. Since the port switch is periodic, in the long run the latter contribution can be averaged, thus yielding a negative average fluid flow rate equal to $V\epsilon/t^*$. As far as the solid motion is concerned, the fixed bed exhibits no movement in the positive direction, but does show a periodic movement in the negative direction, which gives an averaged contribution equal to $V(1-\epsilon)/t^*$. It can be readily seen that the fluid and solids flow rates in the equivalent TCC unit given by Eqs. 19 and 20 correspond exactly to the averaged net effect of the continuous and discrete motions observed in an SMB unit and just described.

Now, let us consider an SMB unit and its nonnegligible extra-column dead volume. First, it is worth observing that trying to find an equivalent TCC configuration with dead volume does not make sense. This would imply the adoption of some unrealistic solid bypass between columns and would also be ineffective, since a new Equilibrium Theory of TCC units with extra-column dead volume would have to be developed. Therefore it is best to look for a TCC configuration *with no dead volume* (so that the whole body of knowledge developed so far about optimal design can be applied in a straightforward way) that is equivalent to an SMB configuration *with extra-column dead volume*. In other words, we look for a new set of conversion rules that substitute the classic ones (Eqs. 19 and 20) used until now for systems where $V_j^D = 0$, $j = 1, \ldots, 4$.

To this end, let us refer to Figure 2a, where the same column in Figure 2b is both preceded and followed by a $V_j^D/2$ dead volume. First, let us calculate the net average fluid flow rate, accounting for both the continuous flow and the discrete jumps due to port switching, which in this case also involves the pre- and post-column dead volumes. The fluid-flow rate in the equivalent TCC unit is given by this net average flow rate

$$Q_j^{\mathrm{TCC}} = Q_j - \frac{V\epsilon_b + V_j^D}{t^*}. \tag{21}$$

The average solid flow rate is the same as in the case where there is no extra-column dead volume, since the latter does not affect the discrete motion of the solid phase itself; thus Eq. 19 applies. Substituting Eqs. 19 and 21 in the definition of m_j^{TCC}, and accounting for Eq. 17, that is, $\overline{m}_j = m_j - m_j^D$, yields the equivalence $m_j^{\mathrm{TCC}} = \overline{m}_j$. This proves that in the general nonlinear case by applying the design criteria developed for TCC units (of which Eqs. 13 to 16 for linear systems, and Eqs. A15 to A18 for stoichiometric Langmuir systems with intermediate desorbent and Figure 4 for nonstoichiometric Langmuir systems, are special cases) to the modified flow-rate ratio $\overline{m}_j$ leads to the correct criteria for SMB units with extra-column dead volume. As already noted, the case of no extra-column dead volume is obtained as a special case of the general relationships by letting $V_j^D = 0$.

Results and Discussion

The theoretical findings reported in the previous section are now discussed and compared with simulation results and experimental data.

The simulations have been run with the model discussed in the second section, using a set of realistic parameters, namely the thermodynamic parameters adopted previously to describe the separation of the enantiomers of an epoxide [1*a*,2,7,7*a*-tetrahydro-3-methoxynaphth-(2,3*b*)-oxirene] on Chiralcel-OD, together with the geometrical parameters of the experimental SMB unit [cf. (Küsters et al., 1995) for the original experimental investigation and (Mazzotti et al., 1997a) for the modeling of the same system]. In particular, the thermodynamic equilibrium is described by a Langmuir isotherm

$$n_i = \frac{H_i c_i}{1 + \sum_{j=A,B} a_j c_j} \qquad i = A, B, \tag{22}$$

where $H_A = 5.38$; $H_B = 3.85$; $a_A = 0.0321$ L/g; $a_B = 0.0174$ L/g; the column volume is $V = 1.662$ cm^3; and the overall void fraction $\epsilon^* = 0.67$. In order to focus on the role of dead volumes, a few operating parameters are held constant in all simulations, namely the feed concentration, $c_A^F = c_B^F = 2.5$ g/L; the switch time, $t^* = 780$ s; and the modified flow-rate

Table 1. Operating Conditions and Calculated Results for SMB Separations of the System Described by Eq. 22

Run	Dead Vol.		Flow Rates (mL/min)				Purity (%)	
	m_D	N_D	Q_1	Q_2	Q_3	Q_4	P_R	P_E
1	0	—	0.381	0.252	0.273	0.191	100	100
2	3	300	0.508	0.379	0.400	0.318	100	100
3	3	1	0.508	0.379	0.400	0.318	99.12	93.76
4	1	1	0.423	0.294	0.316	0.233	100	99.95
5	0.5	1	0.402	0.273	0.295	0.212	100	100

Note: The properties of the extra-column dead volume, that is, m_D and N_D, characterize five different sets of experiments along the segment *AB* in Figure 5 (see Figures 6 to 8 for the corresponding performance). The flow rate and product purity values refer to the operating conditions of point *C* in Figure 5.

ratios in sections 1 and 4, $\overline{m}_1 = 7$ and $\overline{m}_4 = 2.5$. It is worth noting that when changing the extra-column dead volume these two values yield different flow rates in sections 1 and 4, as in Eq. 17. Nevertheless, the preceding choice guarantees that they are at least 20% larger and smaller, respectively, than the corresponding critical value. This choice guarantees complete regeneration of the stationary and mobile phases, respectively, thus making the performance of the SMB depend only on the position of the operating point in the $(\overline{m}_2, \overline{m}_3)$ plane (Storti et al., 1989; Migliorini et al., 1998). In all simulations it has been assumed that all extracolumn dead volumes are the same, that is, $V_j^D = V^D$, $j = 1, \ldots, 4$.

The complete separation region in the $(\overline{m}_2, \overline{m}_3)$ plane for the system under examination is illustrated in Figure 5 (Mazzotti et al., 1997a). Simulations at different values of the extra-column dead volume, V^D, and of the number of mixing stages in the dead volume, N_D (yielding a higher or lesser degree of backmixing in the dead volume), have been carried out for values of the operating parameters corresponding to the points along the segment *AB* in the figure. These simulations can be grouped in five classes, whose features are reported in Table 1 with reference to the representative point *C*, which falls within the complete separation triangle in Figure 5. In particular, the table reports the amount of dead volume considered, m_D, the degree of backmixing in the dead volumes, namely, N_D, and the flow-rate values calculated according to Eq. 17; finally, the calculated values of the product purity also are indicated. It is worth noting that the same $\overline{m}_j$ values yield rather different values of the flow rates for different degrees of dead volume; moreover, larger flow rates are needed to compensate for larger values of the extra-column dead volume and to let the operating point remain within the complete separation region.

This section is organized as follows. First, we analyze the role of extra-column dead volume in the absence of important band-broadening effects, running simulations where plug flow is attained in the dead volume itself; this allows us to assess the theoretical results obtained earlier in the frame of Equilibrium Theory. Secondly, we discuss the role of backmixing in the dead volumes, by also considering the effect of changing the ratio between dead and column volume. Finally, some experimental results obtained in our lab where the extra-column dead volume is about 40% of the column volume are discussed in the light of the previous theoretical findings.

Increased residence time in the chromatographic module

Simulations corresponding to operating points along segment *AB* in Figure 5 have been performed twice: first with no extra-column dead volume (run 1 in Table 1), then with a large amount of dead volume, that is, $V^D = 1.645$ cm^3 corresponding to $m_D = 3$ (run 2 in Table 1). This rather large value of m_D has been selected for illustrative purposes. In the latter case, a large number of mixing stages, namely, $N_D = 300$, has been attributed to each portion of the dead volume (with volume equal to $V^D/2$), so as to minimize backmixing and to allow us to focus on the role of the change in residence time, due to the presence of the dead volume, in the chromatographic module illustrated in Figure 2. Calculations not reported here show that down to $N_D = 30$ the effect of extra-column backmixing is negligible in this case.

The purity performance calculated for the first set of simulations (series 1) is illustrated by the solid lines in Figures 6 and 7 as a function of the $\overline{m}_2$ coordinate of the operating points. As expected, since the chromatographic column efficiency is fairly high, that is, $N_C = 300$, the purity values correspond to those predicted by Equilibrium Theory; hence, raffinate purity in Figure 6 is 100% until the operating point enters the pure extract region, where it quickly drops to about 50%, whereas extract purity in Figure 7 increases until reaching 100%, when the operating point leaves the pure raffinate region and enters the complete separation region and, afterwards, the pure extract region.

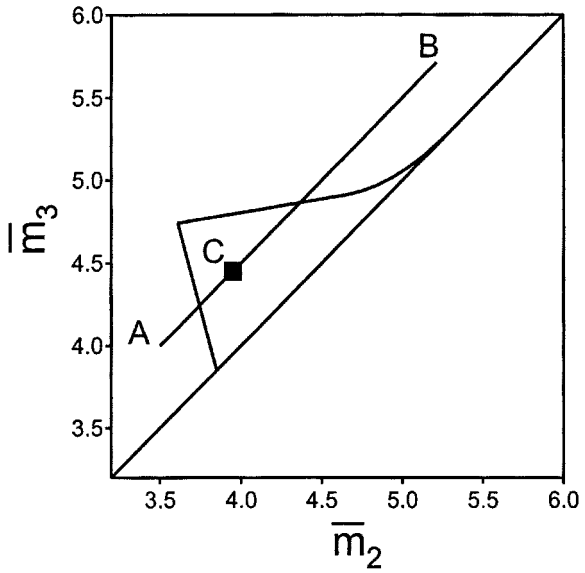

Figure 5. Region of complete separation in the $(\overline{m}_2, \overline{m}_3)$ plane for the system described by Eq. 22; point *C* is (3.95, 4.45).

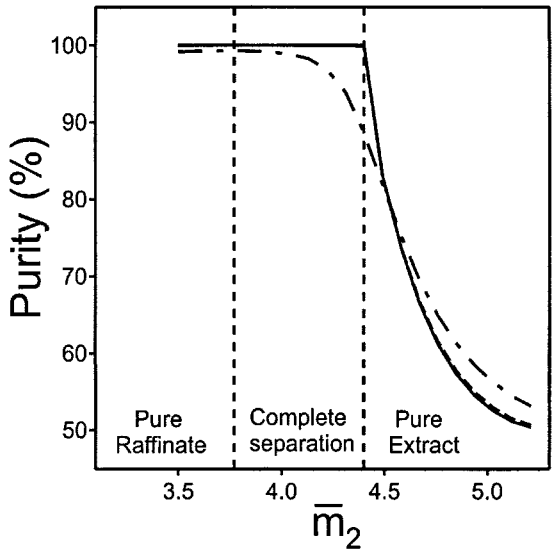

Figure 6. Raffinate purity as a function of $\overline{m}_2$.

Operating conditions as in Figure 5 and Table 1. Series 1: solid line (——); series 2: long-dash line (— —); series 3: dash-dot line (–·–); series 4: dashed line (– – –); series 5: dotted line (· · · ·).

According to the theoretical analysis of the previous section, the separation performance in the second set of simulations (series 2) should be the same, as long as dispersive phenomena are indeed negligible. This is actually confirmed by the calculations, as can be see in Table 1 where the purity values at point *C* coincide for both series 1 and 2, and in Figure 6 and 7 where the curves corresponding to series 2 overlap completely with those of series 1. It is worth pointing out that if operating conditions designed for an SMB *with no* dead volume, such as those corresponding to run 1 in Table 1, were used to operate an SMB *with* dead volume, such as the one in run 2 of Table 1, no separation at all would be achieved and both components would be flushed out through the raffinate port. These calculations prove that this would occur not because of the large amount of backmixing in the dead volume, which in this case is negligible, but because the increased residence time induced by the dead volume had not been properly accounted for. This effect can be exactly and fully accounted for by using the modified flow rate ratios $\overline{m}_j$, as demonstrated in the theoretical section and further shown through the simulations here.

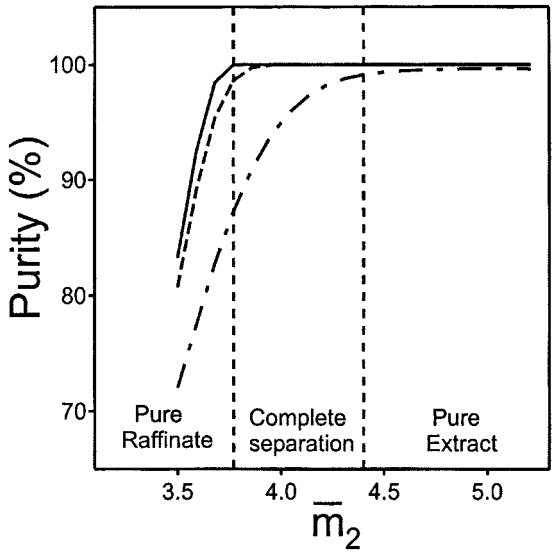

Figure 7. Extract purity as a function of $\overline{m}_2$.

Operating conditions as in Figure 5 and Table 1; symbols as in Figure 6.

Reduced separation efficiency

Simulations corresponding to operating points along segment *AB* in Figure 5 have been repeated in the case of a large dead volume, that is, $m_D = 3$, and strong backmixing in it (series 3 of Table 1). This is obtained by attributing only one mixing stage to each of the two portions of the extracolumn dead volume in Figure 2, which then correspond to two perfectly stirred tanks. As can be observed in Figures 6 and 7 (dot-dashed lines), performance is heavily affected by this backmixing, and purity drops sharply with respect to the situation where plug flow takes place in the dead volume. In particular, in the case of operating point *C* in Figure 5 extract purity drops from 100% to below 94% (see Table 1). These results prove again that the two main effects of extracolumn dead volume can be separated. In fact, also in the absence of extra-column backmixing, there is an increase in the residence time, which can be compensated following the rules given in the third section. On the other hand, the effect of strong extra-column backmixing can be weakened only by minimizing the amount of extracolumn dead volume and the extent of mixing in it.

This last statement is demonstrated by the performance achieved in runs 4 and 5 in Table 1, where the same backmixing effect (only one mixing stage) occurs in a smaller dead volume; in fact, m_D equals 1 and 0.5 in runs 4 and 5, respectively. Purity in the outlet streams increases from the very low values of run 3, where $m_D = 3$, to almost 100% in run 5, thus approaching the ideal situation where the extra-column dead volume is negligible, namely, run 1, where $m_D = 0$, and separation is complete. The same result is illustrated in Figure 6 for the whole set of operating points on segment *AB* in Figure 5 and $m_D = 1$ (series 4 in Table 1, which corresponds to the dashed lines in Figure 6). Extract purity values as a function of $\overline{m}_2$ in Figure 7 are intermediate between those with $m_D = 0$ and $m_D = 3$, whereas raffinate purity in Figure 6 can barely be distinguished from the curve corresponding to no dead volume.

Another viewpoint from which to look at separation performance is provided by the instantaneous concentration profiles in the outlet streams during a period between two successive port switches when cyclic steady state has been achieved. The concentration profiles of component *B* in the raffinate calculated in the five runs reported in Table 1 are shown in Figure 8. Where extra-column band broadening is absent, that is, in runs 1 and 2, the concentration profiles coincide and 100% purity is achieved. Where extra-column back mixing is strong, as in runs 3 to 5, the concentration front is flattened. This effect is small in run 5; in fact, the purity is close to 100%. It is larger in run 4, and even more so

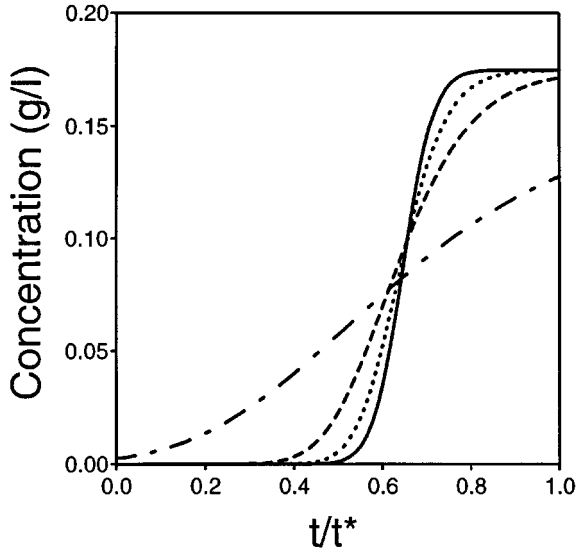

Figure 8. Concentration of component *B* in the raffinate over a period of time t^* after attainment of cyclic steady state.

Operating conditions as in Figure 5 and Table 1; symbols as in Figure 6.

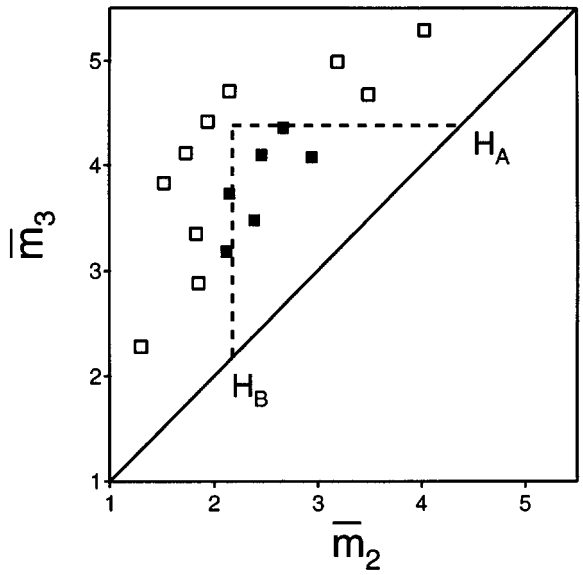

Figure 9. Separation of the Tröger's base enantiomers on CTA (Pedeferri et al., 1999).

Operating points of the experimental runs and linear region of separation in the $(\bar{m}_2, \bar{m}_3)$ plane. The Henry constants for the Tröger's base enantiomers at 323 K are $H_A = 4.38$ and $H_B = 2.18$. Symbols: (□) less than 98% purity in one of the outlet streams; (●) purities greater than 98%.

in run 3, where this phenomenon completely spoils raffinate purity. These results show that all attempts to model the composition profiles in an SMB unit will fail unless a precise description of the behavior in the extra-column dead volume is provided (Yun et al., 1997).

These findings demonstrate that the inhibiting effect of extra-column dead volume on SMB separation performance depends on the size and layout of the dead volume and on the extent of backmixing in it; the role of these two parameters has to be considered with respect to the size of the chromatographic columns and to the retention time in them, which depends on the adsorptivity of the species to be separated.

Experimental results

The theoretical findings presented in the third section and further illustrated in this section, allow us to explain the separation performance achieved in a series of SMB experiments reported by Pedeferri et al. (1999). These experiments refer to the separation of the Tröger's base enantiomers on microcrystalline triacetyl cellulose using ethanol as the mobile phase. The SMB unit has a 2-2-2-2 configuration, with 25-cm-long, 0.46-cm ID columns and $\epsilon^* = 0.56$. The extra-column dead volume is about 40% of the column volume, namely $V_1^D = 1.21$, $V_2^D = 2.30$, $V_3^D = 1.21$, and $V_4^D = 1.76$ cm^3, yielding $m_1^D = 0.66$, $m_2^D = 1.26$, $m_3^D = 0.66$, and $m_4^D = 0.96$, respectively; this is due to the presence of a check valve between each pair of columns.

Sixteen experiments were performed at a racemic feed concentration of 3 g/L; the corresponding operating points in the $(\bar{m}_2, \bar{m}_3)$ plane are shown in Figure 9. The linear complete separation region, taken in this case as a good approximation of the nonlinear triangle (Pedeferri et al., 1999, for further details), is also shown; the nonlinear triangle cannot be calculated exactly due to the non-Langmuirian behavior of the strongly adsorbed enantiomer (Seidel-Morgenstern and Guiochon, 1993; Pedeferri et al., 1999). The closed squares identify operating conditions that achieve complete separation, which is defined as the performance where purity is greater than 98% in both extract and raffinate. Open squares correspond to operating conditions where this requirement is not fulfilled. In particular, points above the linear triangle exhibit poor raffinate purity, whereas poor extract purity is achieved for points on the lefthand side of the triangle [see cf. Pedeferri et al. (1999) for further details]. These results are in rather good agreement with model predictions and prove the correctness of the proposed approach to account for extracolumn dead volumes. As a further confirmation of that, it is worth noting that if the presence of extra-column dead volumes were ignored and Eqs. 13 to 17 with $m_j^D = 0$ were used, then Figure 10, where the operating plane is spanned by m_2 and m_3 and the operating points are shifted upwards along the diagonal with respect to Figure 9, would be obtained. As a consequence, points achieving high product purity in both outlet streams would lie outside the complete separation region, while, on the other hand, points failing to achieve 100% extract purity would lie inside the complete separation region, thus making theoretical predictions and experimental results inconsistent.

Conclusion

The presence of dead space between the fixed beds, whose volume, though minimized, can be comparable to the column volume is a well-known problem of small-scale SMB units made of a series of individual chromatographic columns. In this case, the role of extra-column dead volume can neither be neglected nor considered simply a further source of un-

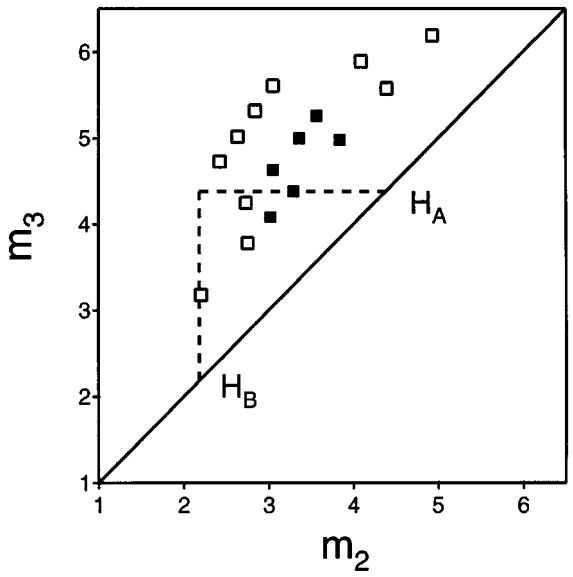

Figure 10. Separation of the Trӧger's base enantiomers on CTA (Pedeferri et al., 1999).

Operating points of the experimental runs and linear region of separation in the (m_2, m_3) plane. Symbols as in Figure 9.

controllable axial dispersion in the unit. In fact, extra-column dead volume yields several effects that are analyzed in this work.

First, dead space increases the residence time of the composition fronts in the chromatographic module made of the dead volume and the chromatographic column. This effect can be exactly accounted for and compensated through an extension of the so-called Triangle Theory, previously developed in the frame of Equilibrium Theory for the robust design of the operating conditions of SMB units. This approach involves the use of the dimensionless modified flow-rate ratios, $\overline{m}_j$, which group together all the key parameters, namely flow rates, switch time, column, and dead volume, and whose optimal values depend only on the parameters of the nonlinear adsorption isotherm used to characterize the system to be separated.

Second, extra-column dead volume yields extra-column band broadening. Our analysis allows us to better understand this effect, thus showing that only when rather severe mixing occurs in the dead volume the correction provided by Equilibrium Theory is not enough to counteract the fact that extracolumn dead volumes somewhat spoil the separation performance. This is clearly shown by detailed model simulations, but cannot easily be predicted *a priori*. Rather practical suggestions can be given to the practitioner, however, namely that equipment components that involve relatively large volumes and therefore mixing, such as check values and pumps, should not be introduced between the columns of the SMB unit, whereas tubings do not matter much, since in the lines, plug-flow conditions are rather closely approached.

Notation

a = Langmuir isotherm parameter
c = fluid-phase concentration
D_{ap} = apparent axial dispersion coefficient
D_D = axial dispersion in the dead volume
f^{eq} = adsorption isotherm
H = Henry constant
K = stoichiometric Langmuir parameter
L = length
L_D = extra-column dead volume length $2 L_D Q/V_D = u$
m = flow-rate ratio
$\overline{m}$ = modified flow rate ratio
n = adsorbed-phase concentration
N = stiochiometric Langmuir parameter
N_D = number of space intervals in the dead volume
N_C = number of space intervals in the column
Q = volumetric flow rate
t = time
t^* = switch time
u = superficial velocity
V = volume of a single chromatographic column
V^D = extra-column dead volume
z = axial coordinate
ϵ^* = overall bed void fraction
ϵ_b = intraparticle void fraction
ϵ_p = interparticle void fraction
ω = equilibrium theory parameter

Subscripts and superscripts

A = more retained compound
B = less retained compound
C = chromatographic column
D = dead volume
i = component index, $i = A, B$
j = section index, $j = 1, \ldots, 4$
r = residence time in the module
R = retention time
s = shock transition
S = desorbent
wf = front flank of a simple wave transition
wr = rear flank of a simple wave transition

Literature Cited

Charton, F., and R. M. Nicoud, "Complete Design of a Simulated Moving Bed," *J. Chromatog. A*, **702**, 97 (1995).

Chiang, A. S. T., "Complete Separation Conditions for a Local Equilibrium TCC Adsorption Unit," *AIChE J.*, **44**, 332 (1998a).

Chiang, A. S. T., "Equilibrium Theory for Simulated Moving Bed Adsorption Processes," *AIChE J.*, **44**, 2431 (1998b).

Gentilini, A., C. Migliorini, M. Mazzotti, and M. Morbidelli, "Optimal Operation of Simulated Moving Bed Units for Non-Linear Chromatographic Separations. II Bi-Langmuir Isotherms," *J. Chromatog. A*, **805**, 37 (1998).

Guiochon, G., S. Golshan-Shirazi, and A. M. Katti, *Fundamentals of Preparative and Nonlinear Chromatography*, Academic Press, New York (1994).

Helferrich, H., and R. Klein, *Multicomponent Chromatography*, Dekker, New York (1970).

Johnson, J. A., and R. G. Kabza, "SORBEX: Industrial-Scale Adsorptive Separation," *Preparative and Production Scale Chromatography*, G. Ganetsos and P. E. Barker, eds., Dekker, New York (1993).

Kniep, H., Vergleich verschiedener verfahrenstechnischer Konzepte zur Durchfürung der präparativen Flüssigchromatographie, PhD Thesis, Otto-von-Guericke-Universität Magdeburg, Germany (1997).

Küsters, E., G. Gerber, and F. D. Antia, "Enantioseparation of a Chiral Epoxide by Simulated Moving Bed Chromatography using Chiralcel-OD," *Chromatographia*, **40**, 387 (1995).

Mazzotti, M., R. Baciocchi, G. Storti, and M. Morbidelli, "Vapor-Phase Simulated Moving Bed Adsorptive Separation of Linear/Nonlinear Paraffins," *Ind. Eng. Chem. Res.*, **35**, 2313 (1996a).

Mazzotti, M., G. Storti, and M. Morbidelli, "Robust Design of Binary Countercurrent Separation Processes: 3. Nonstoichiometric Systems," *AIChE J.*, **42**, 2784 (1996b).

Mazzotti, M., G. Storti, and M. Morbidelli, ''Robust Design of Binary Countercurrent Separation Processes: 2. Multicomponent Systems,'' *AIChE J.*, **40**, 1825 (1994).
Mazzotti, M., G. Storti, and M. Morbidelli, ''Optimal Operation of Simulated Moving Bed Units for Nonlinear Chromatographic Separations,'' *J. Chromatog. A*, **769**, 3 (1997a).
Mazzotti, M., G. Storti, and M. Morbidelli, ''Robust Design of Binary Countercurrent Separation Processes 4. Desorbent in the Feed,'' *AIChE J.*, **43**, 64 (1997b).
Migliorini, C., A. Gentilini, M. Mazzotti, and M. Morbidelli, ''Design of Simulated Moving Bed Units Under Non-Ideal conditions,'' *Ind. Eng. Chem. Res.*, in press (1999).
Migliorini, C., M. Mazzotti, and M. Morbidelli, ''Continuous Chromatographic Separation Through Simulated Moving Beds Under Linear and Nonlinear Conditions,'' *J. Chromatog. A*, **827**, 161 (1998).
Pedeferri, M., G. Zenoni, M. Mazzotti, and M. Morbidelli, ''HPLC-SMB Technology for the Separation of Enantiomers,'' *Chem. Eng. Sci.*, in press (1999).
Rhee, H.-K., R. Aris, and N. R. Amundson, ''On the Theory of Multicomponent Chromatography,'' *Philos. Trans. Roy. Soc. London*, **A267**, 419 (1970).
Ruthven, D. M., and C. B. Ching, ''Counter Current and Simulated Counter Current Adsorption Separation Processes,'' *Chem. Eng. Sci.*, **44**, 1011 (1989).
Seidel-Morgenstern, A., and G. Guiochon, ''Modeling of the Competitive Isotherms and the Chromatographic Separation of Two Enantiomers,'' *Chem. Eng. Sci.*, **48**, 2787 (1993).
Storti, G., R. Baciocchi, M. Mazzotti, and M. Morbidelli, ''Design of Optimal Operating Conditions of Simulated Moving Bed Adsorptive Separation Units,'' *Ind. Eng. Chem. Res.*, **34**, 288 (1995).
Storti, G., M. Masi, S. Carrá, and M. Morbidelli, ''Optimal Design of Multicomponent Countercurrent Adsorption Separation Processes Involving Nonlinear Equilibria,'' *Chem. Eng. Sci.*, **44**, 1329 (1989).
Storti, G., M. Mazzotti, L. T. Furlan, and M. Morbidelli, ''Operation and Design of a Four Part Switching Adsorption Separation Unit,'' *Adsorption Processes for Gas Separation*, F. Meunier and M. D. LeVan, eds., Lavoisier Technique et Documentation, Paris, p. 219 (1991).
Storti, G., M. Mazzotti, L. T. Furlan, M. Morbidelli, and S. Carrá, ''Performance of a Six Port Simulated Moving Bed Pilot Plant for Vapor-Phase Adsorption Separations,'' *Sep. Sci. Technol.*, **27**, 1889 (1992).
Storti, G., M. Mazzotti, M. Morbidelli, and S. Carrá, ''Robust Design and Binary Countercurrent Separation Processes,'' *AIChE J.*, **39**, 471 (1993).
Wu, D.-J., Y. Xie, Z. Ma, and N.-H. L. Wang, ''Design of Simulated Moving Bed Chromatography for Amino Acid Separations,'' *Ind. Eng. Chem. Res.*, **37**, 4023 (1998).
Yun, T., G. Zhong, and G. Guiochon, ''Simulated Moving Bed Under Linear Conditions: Experimental vs. Calculated Results,'' *AIChE J.*, **43**, 935 (1997).

Appendix: SMB—Nonlinear Equilibria

To our knowledge there is only one situation where the system to be separated is characterized by nonlinear adsorption equilibria and the cyclic steady-state solution of the Equilibrium Theory model of a four-section SMB unit (configuration 1-1-1-1, that is, one column per section) under optimal complete separation operating conditions can be calculated exactly. This is the case of the binary separation of species A and B using the desorbent S, where the overall concentration in the fluid phase, namely, $c_{\text{tot}} = c_A + c_B + c_S$, is constant, and the system is characterized by the stoichiometric Langmuir isotherm

$$n_i = \frac{NK_i c_i}{\sum_{j=A,B,S} K_j c_j} \qquad (i = A, B, S), \qquad \text{(A1)}$$

and $K_B < K_S < K_A$, that is, the desorbent exhibits an intermediate adsorptivity with respect to the two components to be separated. In the frame of Equilibrium Theory, each composition state (c_A, c_B, c_S) corresponds to a pair of parameters (ω_1, ω_2) that are calculated by solving the following equation:

$$\sum_{j=A,B,S} \frac{K_j c_j}{K_j - \omega} = 0. \qquad \text{(A2)}$$

Consequently, with reference to Figure 1 the feed stream is characterized by the composition state (c_A^F, c_B^F, c_S^F) corresponding to the pair (ω_H, ω_G), where $K_B < \omega_H \le K_S \le \omega_G < K_A$; and the pure desorbent stream, for which $c_A = c_B = 0$ and $c_S = c_{\text{tot}}$, corresponds to the pair (K_B, K_A) [the reader can refer to Storti et al. (1989, 1993), for a summary of the features of Equilibrium Theory on which the preceding remarks and the following results are based].

The cyclic steady-state solution is composed of constant states separated by transitions, either continuous simple waves or discontinuous shock waves, that propagate along the columns, as illustrated in the physical plane of Figure A1, where the horizontal and vertical coordinate are space and time, respectively [a similar figure was presented by Storti et al. (1991)]. It is worth noting that for the time being it is assumed that the extra-column dead volume is negligible. In particular, four constant states are present: the pure desorbent (S) and the feed state (F), which have already been mentioned, and the E and R states, which are characterized by the ω pairs (K_B, ω_G) and (ω_H, K_A), respectively. The transitions $S \to E$ and $R \to S$ are simple waves with a rear and a front flank, whereas the transitions $E \to F$ and $F \to R$ are shock waves.

Only one time period between two successive switches of the inlet and outlet ports is shown; the new position of the ports at $t = t^*$ is obtained by shifting each port by one column to the right. It can be readily observed that after the switch the composition profile is the same as at time zero, as required by the periodicity of the cyclic steady-state solution. This result is obtained by choosing the four flow rates in the SMB units and the switch time in such a way that the rear side of the simple wave in section 1, the two shock waves in sections 2 and 3, and the front end of the simple wave in section 4 breakthrough at exactly t^*. These conditions can be

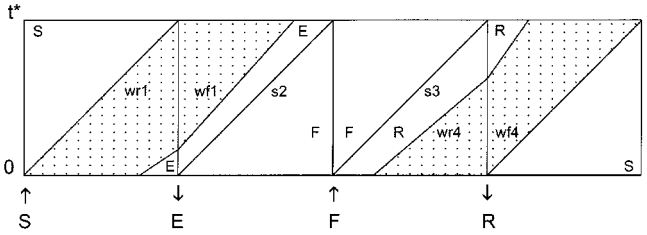

Figure A1. Portrait of the Equilibrium Theory cyclic steady-state solution in the physical plane.

Solid lines s2 and s3 represent shocks, whereas dotted areas correspond to simple wave transitions bracketed by wr1 and wf1 (in sections 1 and 2) and wr4 and wf4 (in sections 3 and 4). The following parameters are used in the calculations: $K_A = 3$, $K_S = 2$, $K_B = 1$. Feed composition: $c_A^F = c_B^F = 0.5$, $c_S^F = 0$. Other parameters are $L = 10$ cm, $\epsilon^* = 0.5$, $t^* = 100$ s.

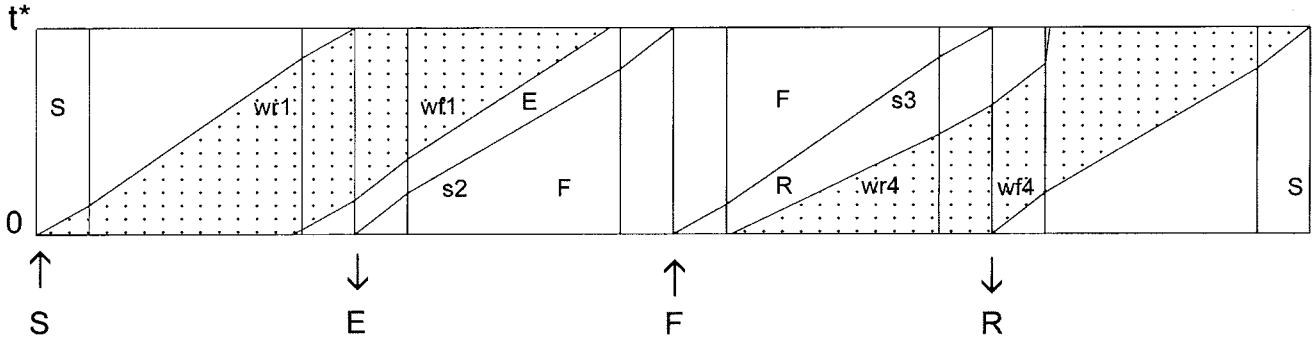

Figure A2. Portrait of the Equilibrium Theory cyclic steady-state solution in the physical plane, in the presence of dead volumes located as shown in Figure 2.

The length of each dead volume column is 2.5 cm, that is, the same for each column, corresponding to $m_j^D = 1$, $j = 1, \ldots, 4$. Other parameters as in Figure A1.

cast in the following mathematical form, where the breakthrough times of interest (see Figure A1) are expressed in terms of either the total derivative Dn_i/Dc_i of each component along the relevant characteristic or the ratio of the change in adsorbed and fluid-phase concentration across the shock, $\Delta n_i/\Delta c_i$ (Storti et al., 1993)

$$\text{Section 1:} \quad t_{wr,1} = \frac{V\epsilon^*}{Q_1}\left[1 + \frac{1-\epsilon^*}{\epsilon^*}\frac{K_A}{K_S}\right] = t^*, \tag{A3}$$

$$\text{Section 2:} \quad t_{s,2} = \frac{V\epsilon^*}{Q_2}\left[1 + \frac{1-\epsilon^*}{\epsilon^*}\frac{\omega_G\omega_H}{K_A K_S}\right] = t^*, \tag{A4}$$

$$\text{Section 3:} \quad t_{s,3} = \frac{V\epsilon^*}{Q_3}\left[1 + \frac{1-\epsilon^*}{\epsilon^*}\frac{\omega_G\omega_H}{K_B K_S}\right] = t^*, \tag{A5}$$

$$\text{Section 4:} \quad t_{wt,4} = \frac{V\epsilon^*}{Q_4}\left[1 + \frac{1-\epsilon^*}{\epsilon^*}\frac{K_B}{K_S}\right] = t^*. \tag{A6}$$

These constraints can be readily recast in terms of the flow-rate ratios m_j defined by Eq. 6 as follows

$$m_1 = \frac{K_A}{K_S}, \tag{A7}$$

$$m_2 = \frac{\omega_G\omega_H}{K_A K_S}, \tag{A8}$$

$$m_3 = \frac{\omega_G\omega_H}{K_B K_S}, \tag{A9}$$

$$m_4 = \frac{K_B}{K_S}. \tag{A10}$$

As anticipated, these constraints correspond to the optimal operating conditions calculated through the Equilibrium Theory by following a different procedure. Although the result is the same as the one obtained through the approach adopted previously (Mazzotti et al., 1997b), however, the procedure followed here can be easily extended to the case where the extra-column dead volume is not negligible.

In fact, in this case the effect of the extra-column dead volume on the residence time in the module illustrated in Figure 2 can be accounted for by the same approach that leads to Eq. 8, that is, by adding the residence time in the dead volume to the breakthrough time of the relevant transition. Therefore, Eqs. A3–A6 have to be written as follows

$$\text{Section 1:} \quad t_{wr,1} + t_1^D = t^*, \tag{A11}$$

$$\text{Section 2:} \quad t_{s,2} + t_2^D = t^*, \tag{A12}$$

$$\text{Section 3:} \quad t_{s,3} + t_3^D = t^*, \tag{A13}$$

$$\text{Section 4:} \quad t_{wf,4} + t_4^D = t^*, \tag{A14}$$

Finally, upon rearrangement, the optimal complete separation operating conditions can be expressed in terms of the modified flow rate ratio defined by Eq. 17

$$\overline{m}_1 = \frac{K_A}{K_S}, \tag{A15}$$

$$\overline{m}_2 = \frac{\omega_G\omega_H}{K_A K_S}, \tag{A16}$$

$$\overline{m}_3 = \frac{\omega_G\omega_H}{K_B K_S}, \tag{A17}$$

$$\overline{m}_4 = \frac{K_B}{K_S}. \tag{A18}$$

The cyclic steady-state solution in the presence of nonnegligible extra-column dead volume is illustrated in Figure A2. It is worth noting that all transitions have the same propagation rate along the dead volume zones, since there is no adsorbent, and hence no chromatographic interaction with it.

Thus summarizing in both the linear and nonlinear cases (at least in the single case where the exact cyclic steady-state solution can be calculated), accounting for the extra-column dead volume leads to a set of constraints on the modified flow-rate ratios $\overline{m}_j$ that are essentially the same as those obtained on the flow-rate ratios m_j when $V_j^D = 0$. The new set of constraints on $\overline{m}_j$ reduce to the ones on m_j wherever the extra-column dead volume is negligible. Unfortunately, these results cannot be extended directly to cases where any kind of nonlinear adsorption isotherm is used. To this end it is necessary to exploit the equivalence between SMB and TCC units, as discussed in the subsection on TCC equivalence.

Manuscript received Oct. 13, 1998, and revision received Apr. 5, 1999.